Mean-field magnetic phase diagram of the periodic Anderson model with the Kondo-compensated phases

Roman Doradziński
Institute of Theoretical Physics, Warsaw University, ulica Hoża 69, 00-681 Warszawa, Poland

Jozef Spałek
Marian Smoluchowski Institute of Physics, Jagiellonian University, ulica Reymonta 4, 30-059 Kraków, Poland
(Received 15 January 1998; revised manuscript received 10 March 1998)

We have determined the ground-state phase diagram for the periodic Anderson model, which comprises both metallic and insulating collinear magnetic phases with compensated magnetic moments. The compensation is due to both the almost-localized character of *f* moments and by an equally important Kondo-type polarization of the conduction electrons; it is effective only close to half filling. In such a situation an antiferromagnetic state with very heavy electrons is formed. Thus we introduce a *true Kondo-lattice* state in a self-consistent manner. The approach is based on the slave-boson method in the saddle-point approximation, in which a strong nonlinear molecular field appears in a natural way. In the polarized state the effective masses are spin dependent. At half filling the *antiferromagnetic Kondo insulator* evolves with increasing hybridization into a *paramagnetic Kondo insulator*. We also predict the existence of a weakly ferromagnetic state (with an extremely small net moment) that can be obtained from the antiferromagnetic heavy-fermion state by applying e.g., pressure. [S0163-1829(98)07929-6]

I. INTRODUCTION

The heavy-fermion state is modelled microscopically by the periodic Anderson model (PAM), and was discussed in both paramagnetic[1] and magnetic[2] cases. The paramagnetic solution encompasses both the almost-localized nature of $4f$ or $5f$ electrons involved, as well as a very strong enhancement of the density of states (DOS) that is independent of the detailed shape of DOS in the bare conduction band. The enhancement is related to an energy scale characterized by *the Kondo temperature* T_K.[1–3] The explicit expression for this temperature resembles that appearing in the impurity Kondo effect;[4] this is one of the reasons why the paramagnetic solution of PAM acquired the name *Kondo lattice state*.[3]

A basic question arises: Can the paramagnetic solution of the Kondo lattice be extended to include the Kondo compensating cloud? A semiquantitative discussion[5] of that point involves a competition between the Ruderman-Kittel-Kasuya-Yosida (RKKY) interaction leading to the magnetic state and the Kondo-cloud formation characterized by the impurity expression for $k_B T_K$. In a more sophisticated approach one determines the instability of paramagnetic KL state (with itinerant electrons) against the spin-density-wave formation.[6] We have calculated explicitly the mean-field magnetic phase diagram of PAM, which includes separately the contributions coming from the negative conduction-electron polarization and the self-screening of *f* electrons. Our approach goes beyond one-boson approach[1] and includes a strong local (single-site) and nonlinear molecular field coming from the *f-f* correlations, which in general cannot be simply related to that coming from RKKY interaction. In construction of the magnetic phases we include the conduction-electron polarization in both heavy-fermion and Kondo-insulating states. We also determine the gap in the latter state. From this analysis the conditions of the Kondo-compensated state formation are specified. In this manner, we extend the well established results[1–3] valid for the paramagnetic phase and determine a *true Kondo-lattice state* in a self-consistent mean-field approximation. Some of the results have been briefly discussed recently.[7]

The structure of this paper is as follows. In Secs. II and III we present respectively a modified version[8] of the spin-rotationally invariant slave boson approach,[9] and define the various collinear-spin magnetic solutions in the saddle-point approximation. In Sec. IV we provide the detailed numerical analysis of magnetic phases and quasiparticle energies in the $T=0$ limit, and comment on the results in physical terms. Finally, in Sec. V we specify the features to be included in order to make the approach applicable to real systems.

II. MODEL AND FORMALISM

We start with the Anderson lattice Hamiltonian in a standard form

$$H=\sum_{i,j,\sigma} t_{ij} c^{\dagger}_{i\sigma} c_{j\sigma} + \varepsilon_f \sum_{i,\sigma} a^{\dagger}_{i\sigma} a_{i\sigma} + V \sum_{i,\sigma} (c^{\dagger}_{i\sigma} a_{i\sigma} + \text{H.c.}) + U \sum_{i} a^{\dagger}_{i\uparrow} a_{i\uparrow} a^{\dagger}_{i\downarrow} a_{i\downarrow}, \tag{2.1}$$

where $c^{\dagger}_{i\sigma}$ and $a^{\dagger}_{i\sigma}$ are the creation operators of the conduction (c) and localized (f) electron states, respectively, t_{ij} is a conduction electrons hopping matrix element, V is the on-site hybridization among c and f electrons, ε_f is the bare *f*-level position, and U is the magnitude of intrasite Coulomb interaction between two f electrons with opposite spins. In

our model calculations we assume that the conduction electron states form a band (spanning from $-W/2$ to $W/2$) with a featureless density of states. This assumption is motivated by the circumstance that the determination of the stable magnetic phases involves a comparison of ground state energies for those phases, which in turn comprises an integration over the filled part of the quasiparticle bands. Those bands contain strong peaks in the density of states caused by hybridization and hence the resultant energies should not depend significantly on details of the bare-band structure.

In the large U limit it is convenient to linearize the dominant Coulomb term. It can be achieved by introducing the slave-boson representation in the rotationally invariant form proposed by Li *et al.*[9]

$$|0,i\rangle = e_i^\dagger |v\rangle, \quad |\sigma,i\rangle = \sum_{\sigma'} \mathrm{P}^\dagger_{i\sigma\sigma'} f^\dagger_{i\sigma'} |v\rangle,$$

$$|2,i\rangle = f^\dagger_{i\uparrow} f^\dagger_{i\downarrow} d_i^\dagger |v\rangle, \tag{2.2}$$

with the 2×2 matrix $\mathrm{P}_{i\sigma\sigma'} = \frac{1}{2}[p_{i0}\mathbb{1} + \mathbf{p}_i\cdot\boldsymbol{\tau}]_{\sigma\sigma'}$. Here $|0,i\rangle$, $|\sigma,i\rangle$, and $|2,i\rangle$ are the empty, singly, and doubly occupied f-level states (at ith lattice site), $|v\rangle$ is an abstract Bose and Fermi vacuum state, $f_{i\sigma}$ is a pseudofermion field, e_i, d_i, and p_{i0} are slave-boson (spin $S=0$) scalar fields, $\mathbf{p}_i$ is a slave-boson ($S=1$) vector field, and $\boldsymbol{\tau}$ denotes the Pauli matrices (τ_x,τ_y,τ_z). In this representation a spin-rotation invariance of Hamiltonian (2.1) is conserved, but the Fock space is considerably enlarged. In order to maintain the physical matrix elements unchanged it is necessary to impose constraints which have been discussed before.[9,7]

As noticed by Spałek and Wójcik,[8] one of the constraints, namely, $\Sigma_\sigma f^\dagger_{i\sigma} f_{i\sigma} = \frac{1}{2}[p^\dagger_{i0}p_{i0} + \mathbf{p}_i^\dagger\mathbf{p}_i] + 2d_i^\dagger d_i$, implies the equivalence between representation of the spin operator of the physical f electron, $\mathbf{S}_i \equiv \frac{1}{2}\Sigma_{\sigma,\sigma'} a^\dagger_{i\sigma}\boldsymbol{\tau}_{\sigma\sigma'}a_{i\sigma'}$, and that of the pseudofermion, $\mathbf{K}_i \equiv \frac{1}{2}\Sigma_{\sigma,\sigma'} f^\dagger_{i\sigma}\boldsymbol{\tau}_{\sigma\sigma'}f_{i\sigma'}$. Therefore it can be rewritten equivalently as

$$\sum_{\sigma,\sigma'} f^\dagger_{i\sigma}\boldsymbol{\tau}_{\sigma\sigma'} f_{i\sigma'} - p^\dagger_{i0}\tilde{\mathbf{p}}_i - \tilde{\mathbf{p}}_i^\dagger p_{i0} = 0, \tag{2.3}$$

where $\tilde{\mathbf{p}}_i = (p_{i1}, -p_{i2}, p_{i3})$. This form of the constraint provides a correct fermion quasiparticle energy in an applied field, and allows for the representation of the spin $\mathbf{S}_i$ in terms of new fermions.

A brief comment on representation (2.2) is in order. First, the second of the states can be written in the spinor representation as

$$|\mathbf{1},\mathbf{i}\rangle = \frac{1}{2}[p^\dagger_{i0}\mathbb{1} + \mathbf{p}_i^\dagger\cdot\boldsymbol{\tau}]\mathbf{f}_i^\dagger|v\rangle, \tag{2.4}$$

where the spinor $\mathbf{f}_i^\dagger = (f^\dagger_{i\uparrow}, f^\dagger_{i\downarrow})$. This is an explicitly rotationally covariant form in the spin space. Thus, any magnetically polarized state can be regarded as breaking SU(2) symmetry. Second, within this representation one can define $\mathbf{S}_i$ as a three-dimensional vector, the circumstance absent in the earlier Kotliar-Ruckenstein representation[10] (the former will reduce to the latter only in the mean-field approximation, in which the dynamics of $S_i^\pm = S_i^x \pm iS_i^y$ disappears).

A radial gauge transformation (for details see Ref. 9) allows us to eliminate the path integration over the phase variables for the fields e_i, p_{i0}, and $\mathbf{p}_i$, which are then transformed into real and nonnegative quantities e_i, q_{i0}, and $\mathbf{q}_i$. Under these circumstances the Lagrange multipliers[9,7] α_i, β_{i0}, and $\boldsymbol{\beta}_i$ transform into time-dependent bosonic fields. Finally, the partition function of the system in the Lagrangian formulation of the statistical field theory takes the form

$$Z \equiv \exp\left(-\frac{F}{k_BT}\right) = \int [\mathcal{D}c][\mathcal{D}f][\mathcal{D}e][\mathcal{D}q][\mathcal{D}d][\mathcal{D}\alpha] \times [\mathcal{D}\beta]\exp\left[\int_0^{1/k_BT}(L_F + L_B)\,d\tau\right], \tag{2.5}$$

where L_F (L_B) is a fermionic (bosonic) part of Lagrangian. In what follows we evaluate Z explicitly in the saddle-point approximation.

III. MEAN FIELD SOLUTIONS

A. Paramagnetic, weak ferromagnetic, and strong ferromagnetic cases

In the mean-field (saddle-point) approximation we regard all the bosonic fields constant in space and time, i.e., $\langle e_i\rangle = e$, $\langle d_i\rangle = d$, etc. The self-consistent saddle-point solution is obtained by minimization of the free energy F with respect to the averaged bosonic variables. Without a loss of generality, for the collinear magnetic phases we can assume that $q_{1i} = q_{2i} = \beta_{1i} = \beta_{2i} = 0$, and redefine the q variables, $q_{\sigma i} = (1/\sqrt{2})\,(q_{0i} + \sigma q_{3i})$, so the results have a similar form to those discussed in Ref. 10.

As noticed in Ref. 10 such an approximation does not lead to the correct results in the $U=0$ limit (as well as in the totally spin-polarized limit). A remedy for this in the Anderson lattice model is to renormalize the hybridization.[7]

Taking the space Fourier transform, the following Lagrangians are obtained:

$$L_F = \sum_{\mathbf{k},\sigma}\left\{c^\dagger_{\mathbf{k}\sigma}\left(\frac{\partial}{\partial\tau} - \mu + \epsilon_{\mathbf{k}}\right)c_{\mathbf{k}\sigma} + \tilde{V}_\sigma(c^\dagger_{\mathbf{k}\sigma}f_{\mathbf{k}\sigma} + \text{H.c.}) + f^\dagger_{\mathbf{k}\sigma}\left(\frac{\partial}{\partial\tau} - \mu + \varepsilon_f + \beta_0 + \sigma\beta_3\right)f_{\mathbf{k}\sigma}\right\} \tag{3.1}$$

and

$$L_B = N\{\alpha(e^2 + d^2 + q_\uparrow^2 + q_\downarrow^2 - 1) - \beta_0(q_\uparrow^2 + q_\downarrow^2 + 2d^2) - \beta_3(q_\uparrow^2 - q_\downarrow^2) + Ud^2\}. \tag{3.2}$$

The equation $\partial F/\partial\alpha = 0$ reduces to a simple condition $e^2 + q_\uparrow^2 + q_\downarrow^2 + d^2 = 1$, which allows for the elimination of e and α. Finally, for the rectangular DOS in the bare conduction band, the explicit expression for the free energy is

$$f \equiv \frac{F}{N} = -\frac{k_B T}{W}\sum_{\sigma,s}\int_{-W/2}^{W/2} \ln[1+e^{-(E_\sigma^{(s)}-\mu)/k_B T}]d\epsilon - \beta_0(q_\uparrow^2+q_\downarrow^2+2d^2) - \beta_3(q_\uparrow^2-q_\downarrow^2) + Ud^2 + \mu n_e , \tag{3.3}$$

where $E_\sigma^{(s)}$ denotes the hybridized subband energies (numbered by $s=\pm 1$)

$$E_\sigma^{(s)} = \frac{1}{2}[\epsilon + \varepsilon_f + \beta_0 + \sigma\beta_3 + s\sqrt{(\epsilon-\varepsilon_f-\beta_0-\sigma\beta_3)^2+4\tilde{V}_\sigma^2}], \tag{3.4}$$

$\tilde{V}_\sigma$ is the renormalized hybridization

$$\tilde{V}_\sigma = V\frac{q_\sigma\sqrt{1-d^2-q_\uparrow^2-q_\downarrow^2}+dq_{-\sigma}}{\sqrt{d^2+q_\sigma^2}\sqrt{1-d^2-q_\sigma^2}}, \tag{3.5}$$

and $n_e = N_e/N$ is the total density of electrons per site. In this paper we vary n_e between 0 and 2. The spin dependence of the quasiparticle energy originates from the molecular field β_3 and renormalization of the hybridization.[11] The remaining equations to be solved are $\partial f/\partial q_\uparrow = \partial f/\partial q_\downarrow = \partial f/\partial d = \partial f/\partial \beta_0 = \partial f/\partial \beta_3 = \partial f/\partial \mu = 0$.

A number of physical quantities can be determined once we know the correlation functions $\langle f_{\mathbf{k}\sigma}^\dagger f_{\mathbf{k}\sigma}\rangle$ and $\langle c_{\mathbf{k}\sigma}^\dagger c_{\mathbf{k}\sigma}\rangle$. Of special interest are: the filling of conduction band (n_c) and f-level states (n_f), and their spontaneous magnetizations (m_c and m_f, respectively), all quantities per site. Under the assumption of the translational invariance of the system, they are expressed as

$$m_f \equiv \frac{1}{N}\sum_{\mathbf{k},\sigma}\sigma\langle f_{\mathbf{k}\sigma}^\dagger f_{\mathbf{k}\sigma}\rangle = q_\uparrow^2 - q_\downarrow^2, \tag{3.6}$$

$$m_c \equiv \frac{1}{N}\sum_{\mathbf{k},\sigma}\sigma\langle c_{\mathbf{k}\sigma}^\dagger c_{\mathbf{k}\sigma}\rangle, \tag{3.7}$$

$$n_f \equiv \frac{1}{N}\sum_{\mathbf{k},\sigma}\langle f_{\mathbf{k}\sigma}^\dagger f_{\mathbf{k}\sigma}\rangle = q_\uparrow^2 + q_\downarrow^2 + 2d^2, \tag{3.8}$$

$$n_c \equiv \frac{1}{N}\sum_{\mathbf{k},\sigma}\langle c_{\mathbf{k}\sigma}^\dagger c_{\mathbf{k}\sigma}\rangle, \tag{3.9}$$

where the total magnetic moment is $m = m_f + m_c$, and the fillings obey the relation $n_f + n_c = n_e$.

Four types of ground states can be determined, namely, (1) paramagnetic (P) for any n_e: $q_\uparrow^2 = q_\downarrow^2$, $\beta_3 = 0$ and $m = 0$, (2) weak ferromagnetic (WF) for $1 < n_e < 2$: $q_\uparrow^2 \neq q_\downarrow^2$, $\beta_3 \neq 0$ and $|m| = 2 - n_e$, (3) strong ferromagnetic (SF) for $1 < n_e \leq 2$: $q_\uparrow^2 \neq q_\downarrow^2$, $\beta_3 \neq 0$ and $|m| > 2 - n_e$, (4) ferromagnetic (F) for $n_e < 1$: $q_\downarrow^2 = d^2 = 0$ and $|m| = n_e$. They will be discussed numerically in the next section.

B. Antiferromagnetic case

In this case, a three-dimensional (3D) cubic lattice with the lattice parameter A is divided into two interpenetrating sublattices A and B, shifted one from another by a vector $\mathbf{R}_{AB} = (a,a,a)$. In general, one can choose $\langle q_{i\sigma}\rangle = q_\sigma^u + \sigma q_\sigma^s \cos \mathbf{Q}\cdot\mathbf{R}_i$, where $\mathbf{Q} = (\pi/a, \pi/a, \pi/a)$, and q^u and q^s are uniform and staggered parts, respectively. If one assumes additionally that neither ferrimagnetism nor charge-density wave are present, then $\langle q_{i\sigma}\rangle = q^u + \sigma q^s \cos \mathbf{Q}\cdot\mathbf{R}_i$. The remaining mean fields are assumed to be $\langle e_i\rangle = e$, $\langle d_i\rangle = d$, $\langle \beta_{0i}\rangle = \beta_0$, $\langle \beta_{3i}^s\rangle = \beta_3^s \cos \mathbf{Q}\cdot\mathbf{R}_i$, i.e., the staggered molecular field β_{3i}^s is the source of the antiferromagnetism. In this picture the f-level magnetization is staggered ($m_{fi} = m_f^s \cos \mathbf{Q}\cdot\mathbf{R}_i$) and the f-level filling is spatially uniform ($n_{fi} = n_f^u$).

The renormalized hybridization can be rewritten in the form $\tilde{V}_{i\sigma} = \tilde{V}^u + \sigma\tilde{V}^s \cos \mathbf{Q}\mathbf{R}_i$, where

$$\tilde{V}^{u,s} = \frac{V}{2}\left[\frac{\sqrt{1-d^2-2(q^u)^2-2(q^s)^2}(q^u+q^s)+d(q^u-q^s)}{\sqrt{d^2+(q^u+q^s)^2}\sqrt{1-d^2-(q^u+q^s)^2}} \pm \frac{\sqrt{1-d^2-2(q^u)^2-2(q^s)^2}(q^u-q^s)+d(q^u+q^s)}{\sqrt{d^2+(q^u-q^s)^2}\sqrt{1-d^2-(q^u-q^s)^2}}\right], \tag{3.10}$$

with the plus sign corresponding to the uniform part $\tilde{V}^u$ and the minus sign corresponding to the staggered part $\tilde{V}^s$. After elimination of e and α the bosonic part of the Lagrangian takes the form

$$L_B = N\{-2\beta_0[(q^u)^2+(q^s)^2+d^2] - 4\beta_3^s q^u q^s + Ud^2\}. \tag{3.11}$$

The fermionic part can be written in a compact form as

$$L_F = \sum_{\mathbf{k}\in RBZ,\sigma}\mathbf{X}_{\mathbf{k}\sigma}^\dagger\left(\frac{\partial}{\partial\tau} - \mu + \mathcal{E}_{\mathbf{k}\sigma}\right)\mathbf{X}_{\mathbf{k}\sigma}, \tag{3.12}$$

where

$$\mathcal{E}_{\mathbf{k}\sigma} = \begin{bmatrix} \varepsilon_f+\beta_0 & \tilde{V}^u & \sigma\beta_3^s & \sigma\tilde{V}^s \\ \tilde{V}^u & \epsilon_{\mathbf{k}} & \sigma\tilde{V}^s & 0 \\ \sigma\beta_3^s & \sigma\tilde{V}^s & \varepsilon_f+\beta_0 & \tilde{V}^u \\ \sigma\tilde{V}^s & 0 & \tilde{V}^u & -\epsilon_{\mathbf{k}} \end{bmatrix}. \tag{3.13}$$

The summation in Eq. (3.12) is running over the reduced (halved) Brillouin zone (RBZ). $\mathbf{X}_{\mathbf{k}\sigma}^\dagger \equiv (f_{\mathbf{k}\sigma}^\dagger, c_{\mathbf{k}\sigma}^\dagger, f_{\mathbf{k}+\mathbf{Q}\sigma}^\dagger, c_{\mathbf{k}+\mathbf{Q}\sigma}^\dagger)$ is a four-component vector. In order to obtain the matrix (3.13), perfect nesting was assumed, i.e., $\epsilon_{\mathbf{k}+\mathbf{Q}} = -\epsilon_{\mathbf{k}}$. For the sake of simplicity, it was also assumed that the bare DOS within the RBZ is also rectangular and spans between $-W/2$ and 0. Finally, the free energy expression for the antiferromagnetic case is

$$f=-\frac{2k_BT}{W}\sum_s \int_{-W/2}^{0} \ln[1+e^{-(E^{(s)}-\mu)/k_BT}]d\epsilon$$
$$-2\beta_0[(q^u)^2+(q^s)^2+d^2]-4\beta_3^s q^u q^s+Ud^2+\mu n_e, \tag{3.14}$$

where $E^{(s)}$ ($s=1,2,3,4$) are the spin-independent eigenvalues of the matrix (3.13) for given ϵ (the reduced band is split into four separate subbands). In effect, the mean-field equations to be solved numerically are $\partial f/\partial q^u=\partial f/\partial q^s=\partial f/\partial d=\partial f/\partial\beta_0=\partial f/\partial\beta_3^s=\partial f/\partial\mu=0$.

As in the previous case, many interesting physical quantities can be drawn from the correlation functions. For example,

$$n_f^u\equiv\frac{1}{N}\sum_{\mathbf{k}\in RBZ,\sigma}[\langle f_{\mathbf{k}\sigma}^\dagger f_{\mathbf{k}\sigma}\rangle+\langle f_{\mathbf{k}+\mathbf{Q}\sigma}^\dagger f_{\mathbf{k}+\mathbf{Q}\sigma}\rangle], \tag{3.15}$$

$$m_f^u\equiv\frac{1}{N}\sum_{\mathbf{k}\in RBZ,\sigma}\sigma[\langle f_{\mathbf{k}\sigma}^\dagger f_{\mathbf{k}\sigma}\rangle+\langle f_{\mathbf{k}+\mathbf{Q}\sigma}^\dagger f_{\mathbf{k}+\mathbf{Q}\sigma}\rangle], \tag{3.16}$$

$$n_f^s\equiv\frac{1}{N}\sum_{\mathbf{k}\in RBZ,\sigma}[\langle f_{\mathbf{k}+\mathbf{Q}\sigma}^\dagger f_{\mathbf{k}\sigma}\rangle+\langle f_{\mathbf{k}\sigma}^\dagger f_{\mathbf{k}+\mathbf{Q}\sigma}\rangle], \tag{3.17}$$

$$m_f^s\equiv\frac{1}{N}\sum_{\mathbf{k}\in RBZ,\sigma}\sigma[\langle f_{\mathbf{k}+\mathbf{Q}\sigma}^\dagger f_{\mathbf{k}\sigma}\rangle+\langle f_{\mathbf{k}\sigma}^\dagger f_{\mathbf{k}+\mathbf{Q}\sigma}\rangle], \tag{3.18}$$

and analogically for the conduction electrons, but with the fields c put in place of f. One obtains easily that $m_f^u=n_f^s=0$, $n_f^u=2(q^u)^2+2(q^s)^2+2d^2$, and $m_f^s=4q^uq^s$. The total staggered moment is defined as $m^s\equiv m_f^s+m_c^s$, and the total density of electrons is $n^u\equiv n_f^u+n_c^u=n_e$. All these quantities are determined numerically and discussed in the next section.

IV. RESULTS OF NUMERICAL ANALYSIS AND DISCUSSION

A. Quasiparticle states and magnetism

In the mean-field approximation we obtain the effective Fermi-liquid picture, in which quasiparticles are of the mixed character, i.e., contain both the itinerant (c) and the localized (f) contributions. In Fig. 1 we plotted schematically the shape of the quasiparticle DOS for each of the phases considered, where the filled parts of the subbands are shaded. In the paramagnetic metal (PM) the density of states, as well as the occupancy of the quasiparticle bands, are the same for both spin directions. The energy gap opens up as a result of the intra-atomic (c-f) hybridization and its magnitude is strongly reduced by the electron correlations. In effect, for $n_e\lesssim 2$ the DOS is strongly enhanced in the vicinity of the Fermi level. For $J\equiv 2V^2U/|\varepsilon_f|(\varepsilon_f+U)\to 0$, the f electrons approach the Mott-localization limit (with $n_f=1$).

In the weakly ferromagnetic metal (WFM) the band structure is no more spin-symmetric;[12] the lower majority-spin band is fully occupied (i.e., contains one electron per site), whereas the minority-spin band remains partially filled (and contains n_e-1 electrons per site), which results in a total moment $|m_c+m_f|=2-n_e$ that is very small for $n_e\to 2$. The natural consequence of this band structure is the spin dependence of many physical quantities, such as the effective mass of electrons.

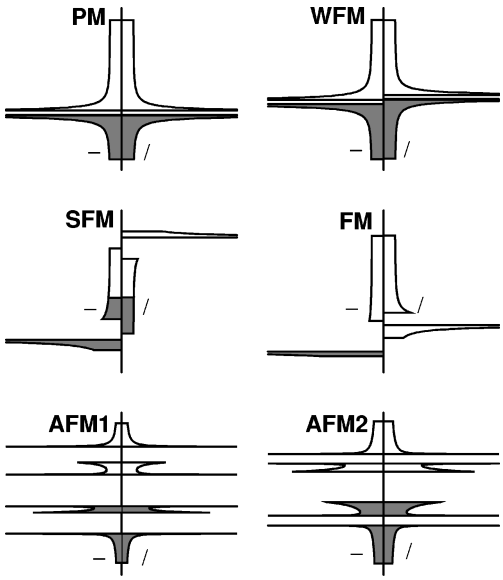

FIG. 1. The quasiparticle band structure for different phases of the mean-field Anderson lattice model. Filled parts of the subbands are shaded.

In contradistinction to the WFM case, the majority-spin electrons of the strongly ferromagnetic metal (SFM) also fill the higher hybridized subband, which results in a stronger polarization of the system; the magnetization is of the order of unity for any $1<n_e\leqslant 2$. SFM remains metallic also in the $n_e=2$ limit.

Ferromagnetic metal (FM) is the phase characteristic for $n_e<1$ region of the phase diagram. One can treat this phase as a continuation of either WFM or SFM, because all these phases are identical for $n_e=1$. In this limit they form a totally polarized ferromagnetic insulator, which is unstable with respect to the antiferromagnetism. In the FM case electrons occupy only one spin subband.

In the antiferromagnetic metallic phases (AFM1 and AFM2) the band structure is more complicated, as it involves four magnetic subbands. As we excluded ferrimagnetism, the subbands are filled to the same extent for both spin directions. We also visualized the basic feature distinguishing between AFM1 and AFM2: their second-lowest subbands are inverted with respect to each other.[13]

An analysis of the self-consistent fields as functions of V allows for a better understanding of the quasiparticle properties and the subband configuration. In Fig. 2 we display the panel with the mean fields for the discussed phases.

Consider first the PM phase, for which $q_\uparrow^2=q_\downarrow^2$ (i.e., $n_{f\sigma}$ is spin independent) and the molecular field β_3 vanishes. The f level is shifted to the position $\tilde{\varepsilon}_f=\varepsilon_f+\beta_0$, and lies inside the conduction band (the renormalization β_0 is of the order of $|\varepsilon_f-\mu|$). With increasing hybridization the energy gap opens up around $\tilde{\varepsilon}_f$, as was discussed by many authors a decade ago.[1–3,14]

In the considered limit $\delta\equiv 2-n_e\ll 1$, the mean fields of the WFM phase are quantitatively very similar to those of

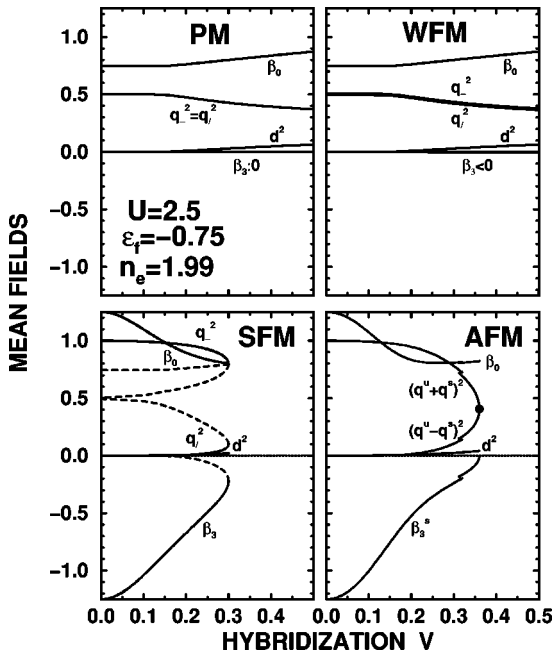

FIG. 2. The mean fields in various phases for $U=2.5$, $\varepsilon_f=-0.75$, and $n_e=1.99$. The AFM plot contains both AFM1 and AFM2 solutions. Dashed lines in the SFM plot represent the lower-magnetization branch. Note that the fields q^2 and d^2 are dimensionless while the fields β are energies (in units of W).

PM, since the moment is extremely small ($m=\delta$). However, the qualitative differences are essential; these are the spin dependence of q_σ^2 and the appearance of a nonzero molecular field β_3. This means that many features of the system, such as the f-level occupancy ($n_{f\sigma}=q_\sigma^2+d^2$), its position ($\tilde{\varepsilon}_f=\varepsilon_f+\beta_0+\sigma\beta_3$), the DOS at the Fermi level, the energy gap, etc., become spin split. Note that the WFM solution does not extend to $V=0$ (with two trivial exceptions, $n_e=2$ and $n_e=1$, as will be shown later in Fig. 11).

The SFM phase is diametrically different: for n_e lying above the critical point (cf. point CP in Fig. 3) there exist two branches of solutions, generating substantially different magnetizations of the system. For the higher-magnetization branch (marked by the solid line) the system is completely polarized ($q_\uparrow^2=1$ and $q_\downarrow^2=d^2=0$) in the $V=0$ limit. Moreover, $\beta_0=-\beta_3$ implying that the majority-spin f level remains unchanged, whereas minority-spin f level is pushed above the Fermi level. With the growing hybridization, the magnetic characteristics of the f subsystem, such as $m_f=q_\uparrow^2-q_\downarrow^2$ and $|\beta_3|$, decrease. The lower-magnetization branch (the dashed lines) tends to the WFM in the small-hybridization limit. With the increasing $|V|$ the magnetization grows and the two branches meet at certain ''critical'' point.

The lower right picture in Fig. 2 describes the AFM phases. The f-electron occupancies of the sublattices {A,B} are $n_f^{A,\sigma}=(q^u+\sigma q^s)^2+d^2$ and $n_f^{B,\sigma}=(q^u-\sigma q^s)^2+d^2$, respectively. Therefore, it is more appropriate to display the fields $(q^u\pm q^s)^2$ instead of $q^{u,s}$. In the $V=0$ limit, only the f level is renormalized (by the term $\beta_0\pm\beta_3^s$), whereas the itinerant electrons remain intact. For $|V|>0$ a new magnetic gap opens up in the conduction band. At the same time, the f levels spread into narrow bands. As the hybridization increases, the second- and third-lowest subbands contract. For $n_e=2$ this process is continuous and for certain V these subbands reduce to the atomic levels. Upon further increasing V, they delocalize again, but the emerging subband structure is inverted with respect to the previous one: the states lying at the top of the subbands are now shifted to the bottom, which manifests itself as an exchange of the divergent parts in DOS shown in Fig. 1. For $n_e<2$ the transition from AFM1 to AFM2 is discontinuous and the middle subbands never reduce to the atomic levels. In the SFM and AFM phases the molecular field β_3 is very strong. In spite of this, the system may have a very small magnetic moment, as discussed next.

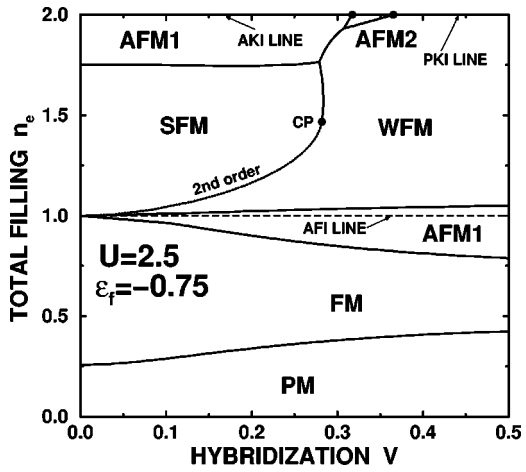

FIG. 3. Magnetic mean-field phase diagram for $U=2.5$ and $\varepsilon_f=-0.75$ (in units of W). Abbreviations are explained in the main text.

B. Magnetic phase diagram

By comparing the ground-state energies of various phases, one can construct the magnetic phase diagram, which comprises the phases listed in Fig. 1. Such a representative diagram on the $V-n_e$ plane is displayed in Fig. 3. The occupancies are $0<n_e\leqslant 2$, and the hybridization is close to the atomic limit (V substantially less than $|\varepsilon_f|$), as only then does one expect spectacular effects associated with the heavy-fermion state and a nontrivial magnetism.

The regions with different magnetic phases form a rather complicated map. For $n_e>1$ it contains both WFM and SFM. Below $n_e=1$ there also exists the entirely polarized FM phase. For not too high hybridization, two antiferromagnetic metallic phases, AFM1 and AFM2, emerge in the vicinity of $n_e=2$, the former being also stable around $n_e=1$. At the bottom of the phase diagram, in the region $0<n_e\lesssim 0.25$, the PM phase becomes the most favorable energetically. There are also two insulating lines: one is the antiferromagnetic-insulator (AFI) line for $n_e=1$, and the second is the $n_e=2$ line, along which *an antiferromagnetic Kondo insulator* (AKI) transforms continuously into *a paramagnetic Kondo insulator* (PKI). The basic feature distinguishing the AKI and AFI phases is the moment compensation occurring in the former case only; this point is discussed in the following subsections.

Almost all quantum-phase-transition lines are of first order and are represented by the solid lines. Only at two points

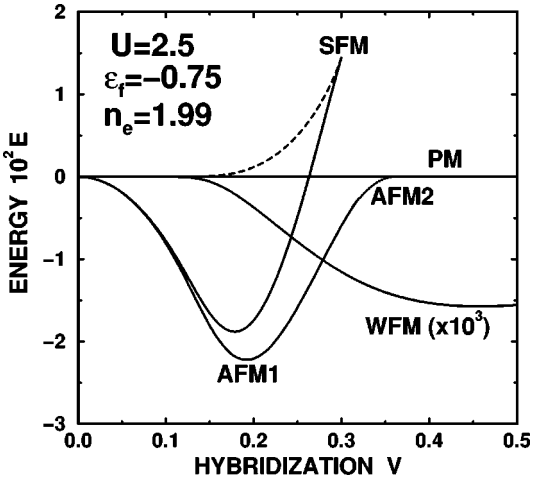

FIG. 4. The energies of all phases existing for $U=2.5$, $\varepsilon_f=-0.75$, and $n_e=1.99$, calculated with respect to PM. The dashed line represents the lower of two SFM branches and the dotted line represents AFM2.

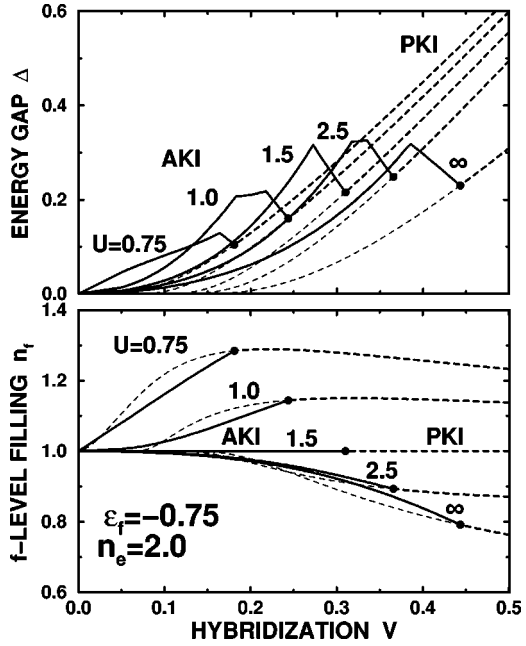

FIG. 5. The hybridization energy gap in the quasiparticle spectrum (top) and the *f*-level occupancy (bottom) for $\varepsilon_f=-0.75$, $n_e=2$, and various U values. The dashed lines are for PKI phase.

on $n_e=2$ line (marked on Fig. 3), and along the line separating SFM and WFM below the critical point (CP), are they continuous.

In order to illustrate the stability conditions of particular phases, we have shown in Fig. 4 their energies calculated with respect to the PM phase. This picture is a cut along the $n_e=1.99$ line of the phase diagram from Fig. 3. Obviously, only the phase with the lowest energy is the stable ground state for given set of parameters (n_e, V, ε_f, U, all energies in units of W). The energy of the WFM state (magnified $\times 10^3$) is very close to that of PM. In the $n_e \to 2$ limit these two phases merge into the PKI state.

The lower branch of the SFM phase (marked by the dashed line) is always less favorable energetically and is included only for the sake of completeness.

C. Kondo-insulator states ($n_e=2$)

In the $n_e=2$ limit we obtain two insulating states denoted as AKI and PKI. In our picture they are the states with totally filled quasiparticle subbands and thus possessing an energy gap Δ between the full and the empty subbands. This parameter is of great importance for the thermodynamic, magnetic, and transport properties. We plotted Δ as a function of hybridization at the top panel of Fig. 5, where the solid lines are drawn for the AKI state and the dashed lines represent the PKI state. The kinks appearing on the former lines are the signs of a changeover in the subband structure. Only in the symmetric case does the band narrowing proceed simultaneously in the two middle subbands (which is a direct consequence of particle-hole symmetry), and a single kink shows up. In the nonsymmetric cases two separate kinks are obtained as the second- and third-lowest subbands are inverted for different V values. At critical V (marked by the solid points), there is a continuous transition to PKI and Δ increases again.

In the PKI case, it can be shown analytically that for $J \ll 1$ the energy gap vanishes exponentially, i.e., $T_K \equiv |\tilde{\varepsilon}_f - \mu| \sim \Delta \sim \tilde{V}^2 \sim d^2 \sim \exp(-((1/2)J)$. This limit is clearly seen in the upper panel of Fig. 5, where the thin-dotted PKI lines merge to the $\Delta=0$ line. At the same time n_f converges to unity, as shown by the thin-dotted lines drawn in the lower panel. However, in our approach PKI is not a stable phase in this region. It must therefore be stressed that the energy gap obtained in our model is not small (cf. Δ in Fig. 5), contrary to the previous discussion, which was limited to the paramagnetic case only.[1] This is a drawback of our mean-field solution. It remains to be seen whether the quantum fluctuations will stabilize the PKI state with $\Delta \to 0$.[15]

Only in the symmetric case is n_f equal to unity in the whole range for both paramagnetic and antiferromagnetic phases. The situation is represented on the bottom panel of Fig. 5 by the solid and dashed lines, respectively. However, as can be seen from this figure, there are no dramatic changes upon U deviating from the symmetric-case value to infinity. In other words, in the wide range of hybridization n_f is still close to unity.

The most important and interesting feature of AKI (justifying its name Kondo insulator) is the magnetic-moment compensation. This effect, obtained here already on the mean-field level of approximation, consists in the compensation of the *f*-electron staggered moment by that of conduction electrons. This compensation is possible because the *f*-electron moment is already strongly reduced from its atomic value by their itineracy induced by the hybridization. The magnetic moments of *f* and *c* electrons are plotted on the top panel of Fig. 6. It should be emphasized that the Kondo-like compensation and the small value of the moments in the limit close to the localization (as expressed by $n_f \to 1$) are the fundamental characteristics of the *magnetic Kondo-lattice state.*

The basic characteristic is also *the compensation ratio* $r \equiv |m_c^s / m_f^s|$. It grows with the increasing hybridization and achieves the maximal value $r_{\max} \approx 1/2$ for the critical value V_c, where AKI transforms continuously into PKI, and where

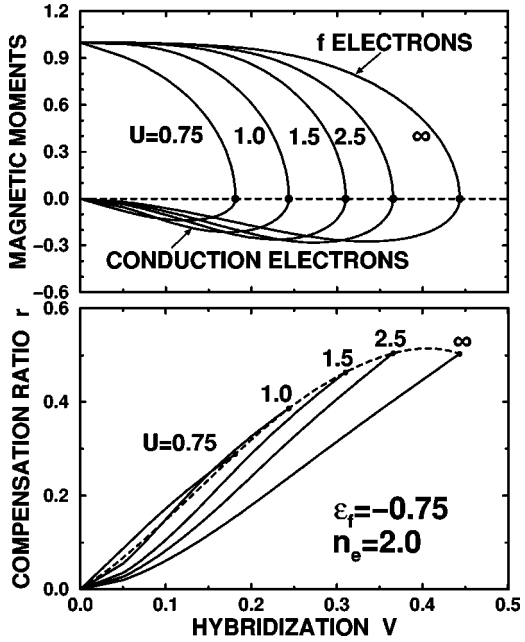

FIG. 6. The magnetic moments of f and conduction electrons (top) and the compensation ratio $r \equiv |m_c^s/m_f^s|$ (bottom) for $\varepsilon_f = -0.75$, $n_e = 2$, and various U values.

m_f^s and m_c^s approach zero as $|V - V_c|^{1/2}$. Both V_c and $r_{\max}$ diminish with decreasing U. This shows that the effect of magnetic-moment compensation and the very existence of the AKI phase are a consequence of the electron correlations present in the system. Contrary to the impurity case, the compensation is never complete.

D. Heavy-fermion states

We consider next the metallic phases with $n_e \lesssim 2$. In Fig. 7 we display the DOS enhancement at the Fermi level for two values of $\delta \equiv 2 - n_e$. The DOS enhancement is equal to the effective mass of the quasiparticles. In the case of stable AFM1 state, the DOS grows with the increasing hybridization through the orders of magnitude. This spectacular

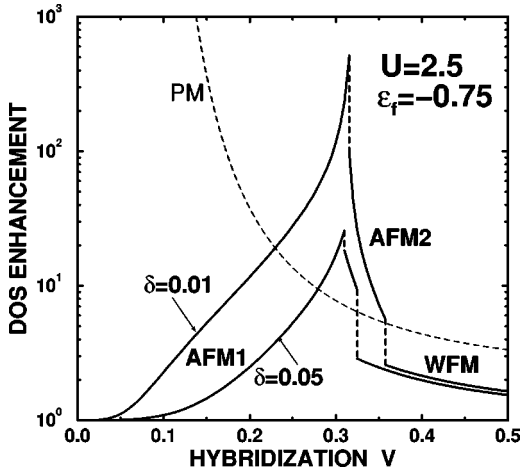

FIG. 7. The DOS enhancement at the Fermi level for $U = 2.5$, $\varepsilon_f = -0.75$, and various dopings $\delta \equiv 2 - n_e$. The transitions from AFM1 to AFM2 and from AFM2 to WFM are discontinuous. The dashed line represents PM phase and is drawn for comparison.

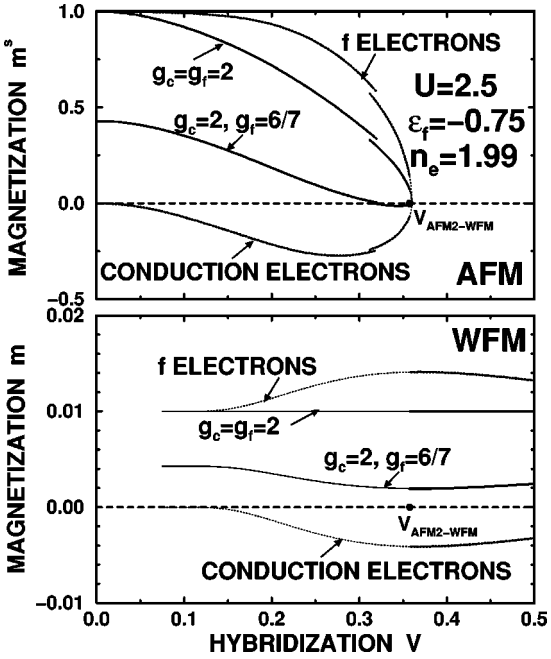

FIG. 8. Staggered magnetization ($m^s \equiv \frac{1}{2} g_f m_f^s + \frac{1}{2} g_c m_c^s$) in AFM1 and AFM2 (top), and uniform magnetization ($m \equiv \frac{1}{2} g_f m_f + \frac{1}{2} g_c m_c$) in WFM (bottom) for $U = 2.5$, $\varepsilon_f = -0.75$, and $n_e = 1.99$. The dotted lines represent the conduction and f-level contributions. $V_{\mathrm{AFM2-WFM}}$ is a discontinuous transition point.

growth reflects the narrowing of the magnetic subbands and the growing contribution of the f states at the Fermi level. After the discontinuous transition to AFM2, the density of states drops sharply and, when the transition to WFM occurs, it attains a value only a few times greater than that in the bare conduction band. For small δ, n_f is essentially the same as in its insulating-state counterpart, presented at the bottom plot of Fig. 5. In contrast, the DOS enhancement for the AFM phases is extremely sensitive to the electron concentration in the system.

Let us stress that the maximal value of DOS is achieved for *intermediate* values of J. In the AFM case the heavy-fermion state is therefore formed only under specific conditions, and should be relatively easily destroyed by applying, e.g., external pressure.

In the PM case (the thin-dashed line) the situation is quite different. In the limit $J \ll 1$ the paramagnetic metal (unstable here) has a highly enhanced DOS, which decreases rapidly with the growing $|V|$.

The moment compensation appears also for $n_e < 2$. In Fig. 8 we plotted the magnetization in three stable phases. In the AFM phases (top) the compensation is nearly the same as in the AKI limit; the AFM1-AFM2 transition is now visible as a discontinuity on the magnetization curve. The total staggered magnetization is defined as $\frac{1}{2} g_f m_f^s + \frac{1}{2} g_c m_c^s$ and has been plotted as solid lines for the two values of Landé factors; among them that for $g_f = \frac{6}{7}$ reflects the situation for the lowest crystal-field doublet of the Ce^{3+} ion. In the WFM phase (bottom) the compensation effect also exists. At the critical value $V_{\mathrm{AFM2-WFM}}$, AFM2 transforms discontinuously into WFM.

In Fig. 9 we characterize the AFM1 and AFM2 phases. AFM1 exists only to the left of the dashed lines. At this border, the second-lowest subband localizes and *the DOS at*

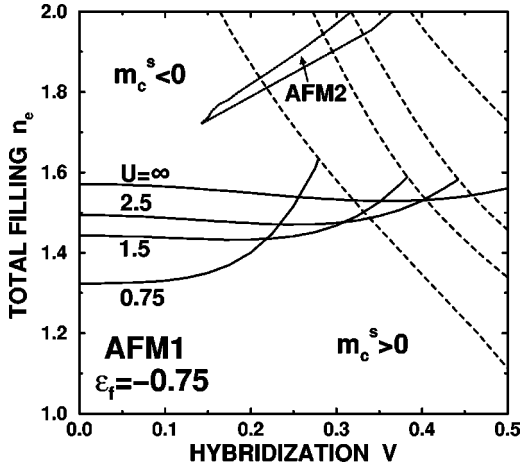

FIG. 9. Above the solid line: the compensated (i.e., with a sign of m_c^s opposite to that of m_f^s) region of AFM1 for $\varepsilon_f=-0.75$ and various U. This phase exists to the left of the dashed lines. The AFM2 phase (the shaded triangle at the top for $U=2.5$) is compensated everywhere.

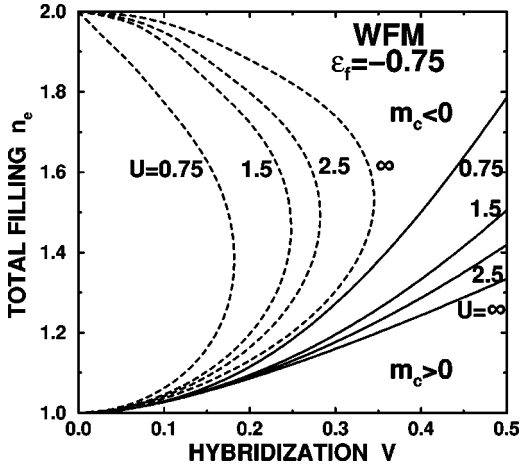

FIG. 11. Above the solid line: the compensated region of WFM for $\varepsilon_f=-0.75$ and various U. This type of mean-field solution exists only to the right of the dashed lines.

the Fermi level diverges. The partial moment compensation occurs only above the solid lines. The AFM2 phase (the shaded area) is compensated everywhere with $r\lesssim 1/2$. The compensation ratio attains the maximal value for $n_e\to 2$.

AFM1 is stable in the vicinity of $n_e=2$ and $n_e=1$. In the latter region the moment is not compensated and the energy gap is relatively large. Hence the limit with $n_e\approx 1$ cannot be regarded as appropriate for the discussion of a *magnetic Kondo-lattice state*.

E. Ferromagnetic region

As we move away from the insulating limit, the AFM state destabilizes with respect to SFM. In Fig. 10 we display the magnetization in both SFM and WFM phases. As previously, the contributions from c and f electrons are represented by the dotted lines. The thin-dashed lines represent the lower of the two SFM branches. A discontinuous transition from SFM to WFM takes place at $V_{\mathrm{SFM-WFM}}$. The moment compensation in the SFM case is far less pronounced (at least by one order of magnitude) than that in the AFM phases near $n_e=2$. It should be also emphasized that the DOS at the Fermi level is not substantially enhanced in SFM, except for n_e very close to unity. For these reasons, the SFM phase cannot be regarded as a good candidate for the Kondo-lattice ground state.

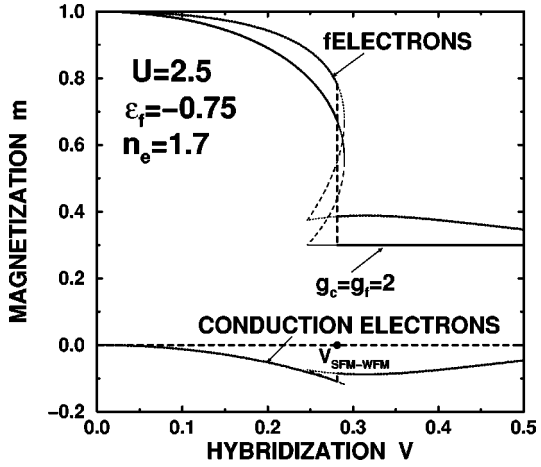

FIG. 10. Uniform magnetization in SFM and WFM for $U=2.5$, $\varepsilon_f=-0.75$, and $n_e=1.7$. Dotted lines represent the conduction and f-level contributions, and dashed lines represent the lower (energetically unfavorable) branch of SFM. Discontinuous transition takes place at $V_{\mathrm{SFM-WFM}}$.

The moment compensation was also determined for the ferromagnetic phases. In Fig. 11 the results for WFM are shown. This type of the mean-field solution exists to the right from the dashed lines. For $n_e=2$ this phase merges into PKI, and for $n_e=1$ it forms a completely polarized FM state. The compensation effect exists only above the solid lines and strengthens with increasing n_e.

V. CONCLUDING REMARKS

Let us summarize briefly the detailed discussion of Secs. II–IV:

(1) Our method of analysis introduces a strong local and nonlinear molecular field (β_3), which *is not* obtained within the standard Gutzwiller approach.[2] It also yields the concept of the spin-dependent effective mass renormalization in the ferromagnetically polarized phases, which is the same for all quasiparticle states.

(2) The Kondo compensation due to the conduction electrons is as important as the f-moment autocompensation due to their itineracy induced by hybridization. These compensations manifest themselves most spectacularly for $n_e\to 2$, where the antiferromagnetic phases are stable. Therefore, our picture involves a competition between itineracy of f electrons and the f-f kinetic exchange on one side, and the concomitant Kondo compensation of staggered moments on the other.

(3) Both the antiferromagnetic and ferromagnetic states with extremely small moments ($\mu_{\mathrm{eff}}\sim 10^{-2}\mu_B$) are possible for $\delta\equiv 2-n_e\ll 1$. One can transform the former into the latter by applying, e.g., pressure.

(4) One should note that the heavy-fermion state with an almost integer valency ($n_f \to 1$), small staggered moment $\mu_{\rm eff} < 0.1\mu_B$, and a large DOS is possible at the same time. It is much more difficult to obtain a stable paramagnetic heavy-fermion state within the periodic Anderson model. The question of whether the quantum fluctuations would stabilize the PM state on expense of the magnetic states, remains open. Related to this is the occurrence of a small gap in the paramagnetic Kondo insulating state.[16]

The present approach represents probably the most general type of mean-field approach taking into account local magnetic correlations among *itinerant* (albeit almost localized) *f* electrons if the Fermi-liquid state is stable. However, two principal factors have been neglected. The first of them is the crystal-field structure of, e.g., the Ce ion[17] in the (3+)-valency state (we have put $g_f = 6/7$ in an *ad hoc* manner). The second of them is the **k** dependence of the hybridization matrix element *V*, which should be included in some cases. Nonetheless, one should emphasize that the true Kondo insulating state is not possible if $V_{\mathbf{k}}$ has zeros at some points on the Fermi surface.

ACKNOWLEDGMENTS

The authors acknowledge the financial support of the KBN grant No. 2P03B 129 12. Conversations with our colleagues K. Byczuk, B. Coqblin, C. Lacroix, M. Lavagna, and A. M. Oleś have been very helpful during the work on this paper.

[1] N. Read and D. Newns, J. Phys. C **16**, L1055 (1983); P. Coleman, Phys. Rev. B **28**, 5255 (1983); **35**, 5072 (1987); Z. Tesanovic and O. T. Valls, *ibid.* **34**, 1918 (1986); A. J. Mills and P. A. Lee, *ibid.* **35**, 3394 (1987). For a comparative study of various mean-field approaches see F. Gebhard, *ibid.* **44**, 992 (1991).

[2] T. M. Rice and K. Ueda, Phys. Rev. B **34**, 6420 (1986); S. Doniach, *ibid.* **35**, 1814 (1987); P. Fazekas and E. Müller-Hartmann, Z. Phys. B **85**, 285 (1991); F. J. Ohkawa, Prog. Theor. Phys. Suppl. **108**, 209 (1992); P. J. Schlottmann, Phys. Rev. B **54**, 12 324 (1996).

[3] For a review see P. A. Lee, T. M. Rice, J. W. Serene, L. J. Sham, and J. W. Wilkins, Comments Condens. Matter Phys. **12**, 99 (1986); D. M. Newns and N. Read, Adv. Phys. **36**, 799 (1987); P. Fulde, J. Keller, and G. Zwicknagl, in *Solid State Physics*, edited by H. Ehrenreich and D. Turnbull (Academic, New York, 1988), Vol. 41, pp. 1–150; N. Grewe and F. Steglich, in *Handbook on the Physics and Chemistry of the Rare Earths* (North Holland, Amsterdam, 1990), Vol. 14, pp. 1ff.

[4] O. Gunnarsson and K. Schöhammer, Phys. Rev. B **28**, 4315 (1983).

[5] S. Doniach, Physica B **91**, 231 (1977). The effective picture coming from the competition of the Kondo effect with the short-range antiferromagnetic correlations has been presented in B. Coqblin *et al.*, J. Phys. Soc. Jpn. **65**, Suppl. B, 64 (1996); J. Arispe, B. Coqblin, and C. Lacroix, Physica B **206–207**, 255 (1995); J. R. Iglesias, C. Lacroix, and B. Coqblin, Phys. Rev. B **56**, 11 820 (1997).

[6] See S. Doniach, Phys. Rev. B **35**, (1987); F. J. Ohkawa, Prog. Theor. Phys. Suppl. **108**, 209 (1992).

[7] R. Doradziński and J. Spałek, Phys. Rev. B **56**, R14 239 (1997).

[8] J. Spałek and W. Wójcik, in *Spectroscopy of Mott Insulators and Correlated Metals*, edited by A. Fujimori and Y. Tokura (Springer-Verlag, Berlin, 1995), pp. 41–65.

[9] T. Li, P. Wölfle, and P. J. Hirschfeld, Phys. Rev. B **40**, 6817 (1989); R. Frésard and P. Wölfle, Int. J. Mod. Phys. B **6**, 685 (1992); **6**, 3087(E) (1992).

[10] G. Kotliar and A. E. Ruckenstein, Phys. Rev. Lett. **57**, 1362 (1986). This method has been applied to the hybridized models in C. A. Balseiro, M. Avignon, A. G. Rojo, and B. Alascio, *ibid.* **62**, 2624 (1989).

[11] Such a renormalization does not provide a proper form of the dynamic spectral function, but is sufficient for a discussion of static properties.

[12] A. M. Reynolds, D. M. Edwards, and A. C. Hewson, J. Phys. C **4**, 7589 (1992).

[13] The two antiferromagnetic phases have been considered also by V. Dorin and P. Schlottmann, Phys. Rev. B **46**, 10 800 (1992); P. Schlottmann, *ibid.* **54**, 12 324 (1996).

[14] N. Read, D. M. Newns, and S. Doniach, Phys. Rev. B **30**, 3841 (1984).

[15] J. Karbowski, Phys. Rev. B **54**, R728 (1996).

[16] The gap is reduced strongly with the increasing temperature, see, e.g., C. Sanchez-Castro, K. S. Bedell, and B. R. Cooper, Phys. Rev. B **47**, 6879 (1993); M. F. Hundley, J. D. Thompson, P. C. Canfield, and Z. Fisk, Physica B **199&299**, 443 (1994); P. S. Riseborough, Phys. Rev. B **45**, 13 984 (1992).

[17] The degenerate structure of PAM (for PM phase) has been treated in K. Yamada, K. Yosida, and K. Hanzawa, Prog. Theor. Phys. Suppl. **108**, 141 (1992); the corresponding situation for Kondo insulators has been analyzed in Yu. Kagan, K. A. Kikoin, and N. V. Prokofév, Pis'ma Zh. Eksp. Teor. Fiz. **57**, 584 (1993) [JETP Lett. **57**, 600 (1993)]; for details see H. Ikeda and K. Miyake, J. Phys. Soc. Jpn. **65**, 1769 (1996).